communications biology

Article

https://doi.org/10.1038/s42003-024-06960-6

The antisense lncRNA of *TAB2* that prevents oxidative stress to enhance the follicular growth in mammals

Nian Li[1,4], Bing Yun[1,4], Liqing Zeng[1], Yuanyuan Lv[1], Yinqi Zhou[1], Ming Fang[1], Shuo Li[1], Yongcai Chen[1], Enyuan Huang[1], Liuhong Zhang[1], Yao Jiang[1,2], Hao Zhang[1], Jiaqi Li[1] ✉ & Xiaolong Yuan[1,3] ✉

LncRNAs are highly implicated in oxidative stress (OS) during the growth of mammalian follicles. *TAK1* binding protein 2 gene (*TAB2*) has been suggested to involve in the normal apoptosis and proliferation of granulosa cells (GCs), the main supporting cells in ovarian follicles. In this study, we found that *TAB2* increased the expressions of *SOD1*, *P50*, and *P65* to suppress the OS, thereby inhibiting the apoptosis and promoting the proliferation in GCs. Notably, *DNMTs* appeared to mediate the expression of *TAB2* without the changes of DNA methylation at *TAB2*'s promoter. We identified an antisense lncRNA of *TAB2*, discovered that DNA methylation regulated the transcription of *TAB2-AS* in GCs, and found *TAB2-AS* medicated the follicular growth of ovaries in vivo. Mechanistically, the hypomethylation of the CpG site (−1759/−1760) activated the transcription of *TAB2-AS*, and the 1–155 nt and 156-241 nt of *TAB2-AS* were respectively complementary to 4368–4534 nt and 4215–4300 nt of *TAB2*'s mRNA to increase the expression of *TAB2*. Moreover, *TAB2-AS* inhibited the OS and apoptosis of GCs, while promoted the proliferation of GCs to expedite the follicular growth, which was in line with that of *TAB2*. Collectively, these findings revealed the antisense lncRNA mechanism mediated by DNA methylation, and *TAB2-AS* might be the target to control OS during follicular growth in mammals.

Many studies have shown that the intracellular oxidative stress (OS) caused by the excess accumulation of reactive oxygen species (ROS) regulates the tissue growth[1] and diseases[2,3] of mammals via inducing cell apoptosis DNA[4,5]. In humans, the superfluous ROS promotes the apoptosis of osteoblast through enhancing OS, thereby causing Aluminum-related bone diseases[6]. Moreover, ROS enhances the apoptosis of human head and neck cancer cells to inhibit the development of head and neck cancer[7]. As the basic structural and functional unit of mammalian ovaries, the follicles are composed of oocytes, granulosa cells (GCs), and membrane cells[8], in which GCs regulate follicular growth and ovulation via mediating the maturation of oocytes[9]. The normal differentiation and proliferation of GCs ensure the growth of ovarian follicles[10], while the excessive apoptosis of GCs decreases the synthesis of extracellular matrix in follicular fluid to induce follicular atresia in mammals[11]. Notably, the OS has been confirmed to be closely related to the follicular growth and ovarian diseases including age-related ovarian dysfunction and ovarian endometriosis[12]. However, the specific mechanisms by which the OS regulates follicular growth through influencing the apoptosis of GCs remain unclear in mammals.

The long non-coding RNAs (lncRNAs) are identified as transcripts that are longer than 200 nt[13], and they are found to be associated with the follicular growth of mammalian ovaries[14,15]. Differentiation antagonizing non-protein coding RNA (*DANCR*) counteracts the human premature ovarian insufficiency via inhibiting the *P53*-dependent GCs aging[16]. In ovine ovaries, follicular development-associated lncRNA (*FDNCR*) promotes the transactivation of decorin (*DCN*) by targeting miR-543-3p, resulting the enhancement of GCs apoptosis and inhibition of follicular growth[17]. The DNA methylation is an important epigenetic modification by which controlled mainly by DNA methyltransferases (*DNMTs*)[18], and regulates the transcription and expression of genes via altering chromatin structure[19,20]. The DNA hypermethylation suppresses the expressions of transcriptional regulators *ID2* and *ID4* during the differentiation of human oligodendrocyte precursor cells via decreasing the activation of promoter[21]. Notably, the

[1]Guangdong Laboratory of Lingnan Modern Agriculture, National Engineering Research Center for Breeding Swine Industry, State Key Laboratory of Swine and Poultry Breeding Industry, Guangdong Provincial Key Laboratory of Agro-Animal Genomics and Molecular Breeding, College of Animal Science, South China Agricultural University, Guangzhou, Guangdong, 510642, China. [2]School of Medical, Molecular and Forensic Sciences, Murdoch University, Murdoch, WA, 6149, Australia. [3]Centre for Healthy Ageing, Health Futures Institute, Murdoch University, Murdoch, WA, 6150, Australia. [4]These authors contributed equally: Nian Li, Bing Yun. ✉e-mail: jqli@scau.edu.cn; yxl@scau.edu.cn

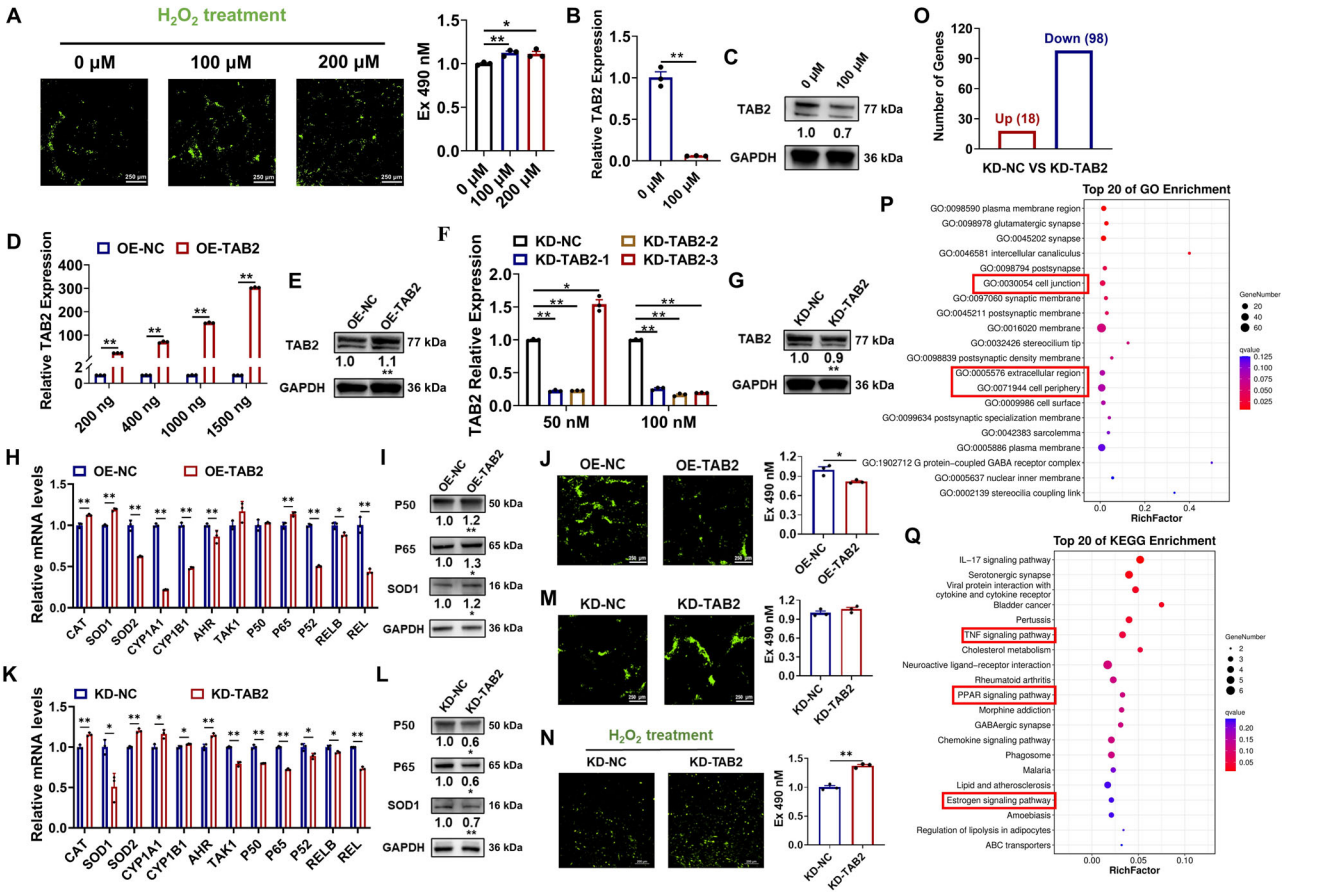

Fig. 1 | *TAB2* activates NF-κB pathway to inhibit the oxidative stress in ovarian GCs. **A** The level of ROS accumulation in ovarian GCs after treating with H_2O_2. The mRNA (**B**) and protein (**C**) expressions of *TAB2* in GCs after treating with H_2O_2. The overexpression efficiencies of the mRNA (**D**) and protein (**E**) of *TAB2*. The knockdown efficiencies of the mRNA (**F**) and protein (**G**) of *TAB2*. The mRNA (**H**) and protein (**I**) expressions of several OS-related and NF-κB pathway genes after overexpression of *TAB2* in GCs. **J** The effects of *TAB2* overexpression on ROS accumulation in GCs. The mRNA (**K**) and protein (**L**) expressions of several OS-related and NF-κB pathway genes in after knockdown of *TAB2* in GCs. **M** The effects of *TAB2* knockdown on the ROS accumulation in GCs. **N** The ROS accumulation in GCs treated with H_2O_2 after knockdown of *TAB2*. **O** The number of differentially expressed genes between KD-NC and KD-TAB2. The GO (**P**) and KEGG (**Q**) results of differentially expressed genes. The scale bars in (**A**, **J**, **M**), are 250 μm, and the scale bars in (**N**) are 200 μm.

hypomethylation of porcine R-spondin 2 (*RSPO2*) promoter enhanced the transcription of *RSPO2* to advance the proliferation of ovarian GCs[22], suggesting that the DNA methylation might play an important role in growth of follicles[14,15,23]. However, the functional mechanism of lncRNAs that are regulated by DNA methylation in the growth of ovarian follicles remains to be investigated.

TAK1 binding protein 2 gene (*TAB2*) is a member of TAB family[24], which arouses the activation of nuclear factor kappa-B (NF-κB) signaling pathway via activating *TAK1* kinase[25,26]. Interestingly, the NF-κB transcription factors have been shown to play a vital role in the follicular growth of mammals through regulating the function of ovarian GCs[27,28]. In mice, the high expressions of NF-κB/P50 and NF-κB/P65 proteins inhibit the follicular atresia via inducing the proliferation of ovarian GCs[29,30]. Moreover, the NF-κB is a pivotal molecular signaling pathway for the regulation of OS[31,32]. The activation of NF-κB pathway inhibits the OS from alleviating the oxidative damage of porcine intestinal epithelial cells[33]. Nevertheless, the specific regulation mechanisms that *TAB2* involves in NF-κB signaling pathway to regulate the follicular growth remain to be further explored. Using cultured GCs, we found that *TAB2* might involve the OS, apoptosis, and proliferation, thereby regulating the follicular growth in ovaries. Ulteriorly, TAB2 antisense RNA (*TAB2-AS*), a lncRNA was identified for *TAB2*, and the specific mechanisms by which DNA demethylation upregulated the expressions of *TAB2* and *TAB2-AS* were further revealed. Our results characterize a promising mechanism regarding the therapeutic benefit of DNA methylation and lncRNA in OS for mammalian follicular growth.

Results

TAB2 activates NF-κB pathway to counteract OS of ovarian GCs

To explore the effects of *TAB2* on OS in ovarian GCs, GCs were treated by hydrogen peroxide (H_2O_2), an inducer of OS. We found that the accumulation of ROS in GCs treated with 100 μM and 200 μM H_2O_2 were increased significantly (Fig. 1A). There was no significant difference between GCs treated with 100 μM and 200 μM of H_2O_2 in the accumulation of ROS (Fig. 1A). Considering the tolerance of GCs and cytotoxicity of H_2O_2, H_2O_2 at a concentration of 100 μM was selected for subsequent experiments. 100 μM H_2O_2 significantly inhibited the mRNA (Fig. 1B) and protein (Fig. 1C) expressions of *TAB2* in GCs. We then markedly increased the mRNA (Fig. 1D) and protein (Fig. 1E) levels of TAB2 (OE-TAB2) in GCs using the overexpression vector of *TAB2*, and 1500 ng/mL of vector showed the greatest effect. Three siRNAs of *TAB2* were synthesized, and 100 nM siRNA2 decreased the mRNA (Fig. 1F) and protein (Fig. 1G) levels of *TAB2* with the strongest knockdown efficiency.

Moreover, we analyzed the mRNA and protein levels of OS-related genes and NF-κB signaling pathway-related genes in GCs after overexpression and knockdown of *TAB2*. The *TAB2* overexpression significantly promoted the mRNA expressions of catalase (*CAT*), superoxide dismutase 1 (*SOD1*), and *P65* (Fig. 1H), and the protein counts of P50, P65, and SOD1 (Fig. 1I), as well as inhibiting the ROS accumulation of GCs (Fig. 1J). Correspondingly, *TAB2* knockdown significantly decreased the mRNA (Fig. 1K) and protein (Fig. 1L) expressions of *P50*, *P65*, and *SOD1*, and increased the ROS accumulation of GCs (Fig. 1M).

Similarly, the *TAB2* knockdown significantly decreased the tolerance of GCs to H_2O_2 induced ROS accumulation (Fig. 1N).

Moreover, we further explored the transcriptomic changes of GCs treated with *TAB2* knockdown, and 116 differentially expressed genes, e.g., prostaglandin D2 receptor (*PTGDR*), matrix metallopeptidase 1 (*MMP1*), and matrix metallopeptidase 9 (*MMP9*) were obtained, compared with control group (Fig. 1O, Table S1). The Gene Ontology (GO) analysis of these differentially expressed genes enriched in cell junction, extracellular region, and cell periphery (Fig. 1P, Table S2), and the Kyoto Encyclopedia of Genes and Genomes (KEGG) analysis showed that these genes enriched in TNF signaling, PPAR signaling, and Estrogen signaling pathways (Fig. 1Q, Table S3), which are highly related to functions of GCs. These results suggested that *TAB2* suppress the OS in ovarian GCs.

TAB2 inhibits the apoptosis but promotes the proliferation of GCs

Ulteriorly, we found that *TAB2* overexpression significantly decreased the mRNA (Fig. 2A) and protein (Fig. 2B) expressions of cysteine aspartic acid specific protease 9 (*Caspase-9*) and *BCL-2* interacting mediator of cell death (*BIM*) of apoptosis-related genes, and the apoptosis levels of GCs (Fig. 2C). *TAB2* knockdown was likely to recover the mRNA (Fig. 2D) and protein (Fig. 2E) expressions of *Caspase-9* and *BIM*, as well as the apoptosis of GCs (Fig. 2F). In addition, *TAB2* overexpression significantly enhanced the mRNA (Fig. 2G) and protein (Fig. 2H) expressions of proliferating cell nuclear antigen (*PCNA*) and cyclin E1 (*CCNE1*) that were the cell proliferation-related genes in GCs, and significantly increased the proliferation rate of GCs (Fig. 2I). Oppositely, *TAB2* knockdown significantly weakened the mRNA (Fig. 2J) and protein (Fig. 2K) expressions of *PCNA* and *CCNE1* in GCs, and significantly decreased the proliferation rate of GCs (Fig. 2L). These results indicated that *TAB2* might prevent OS, and thus inhibit the apoptosis but promote the proliferation of ovarian GCs.

An antisense lncRNA *TAB2-AS* was identified for *TAB2*

5-Aza-CdR, an *DNMTs* inhibitor, was found to significantly increase the mRNA (Fig. 3A) and protein (Fig. 3B) levels of *TAB2*. Similarly, the

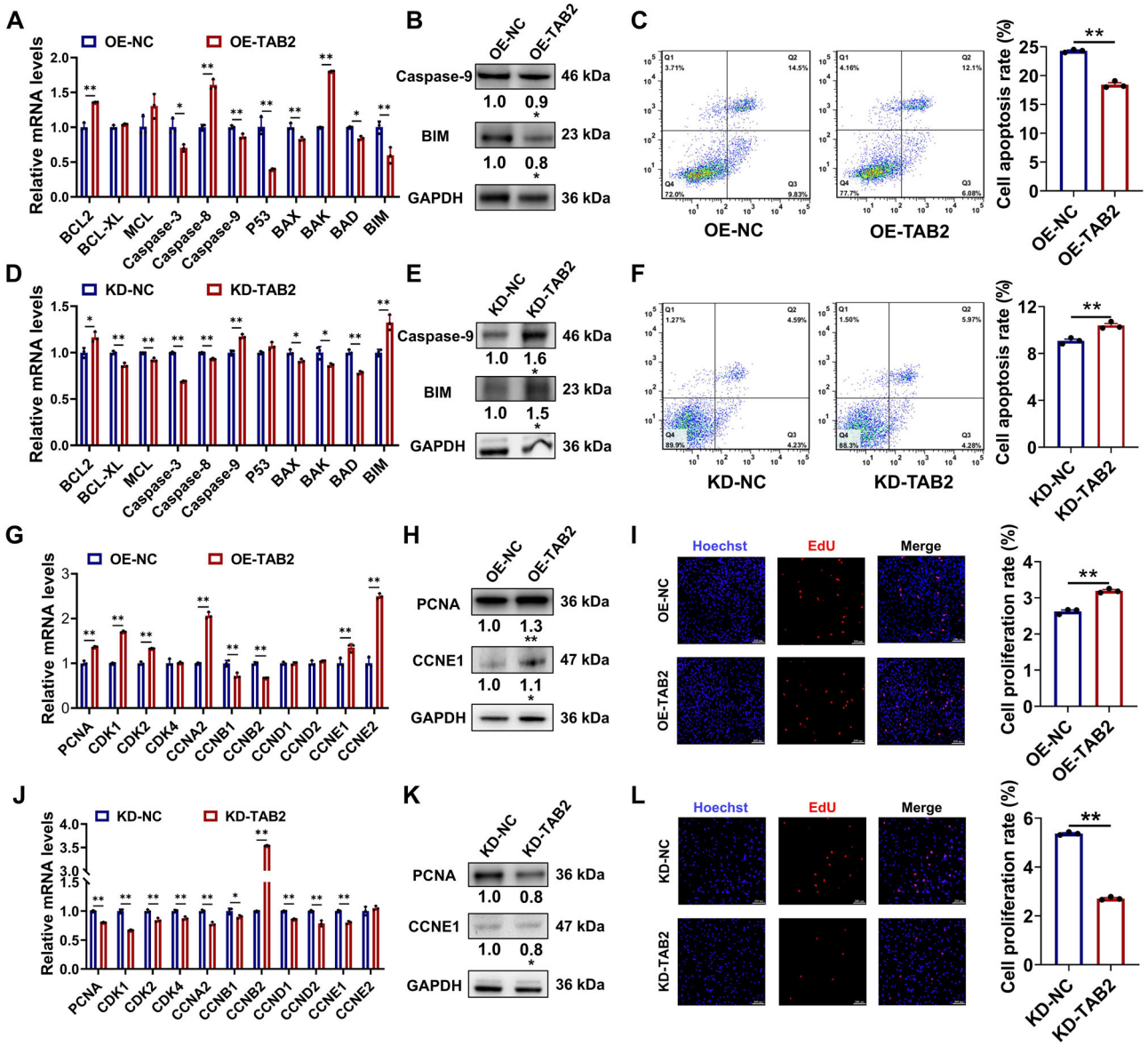

Fig. 2 | *TAB2* inhibits the apoptosis but promotes the proliferation of GCs. The mRNA (**A**) and protein (**B**) expressions of apoptosis-related genes treated with *TAB2* overexpression in GCs. **C** The effect of *TAB2* overexpression on the apoptosis of GCs. The mRNA (**D**) and protein (**E**) expressions of apoptosis-related genes treated with *TAB2* knockdown in GCs. **F** The effect of *TAB2* knockdown on the apoptosis of GCs. The mRNA (**G**) and protein (**H**) expressions of proliferation-related genes treated with *TAB2* overexpression in GCs. **I** The effect of *TAB2* overexpression on the proliferation of GCs. The mRNA (**J**) and protein (**K**) expressions of proliferation-related genes treated with *TAB2* knockdown in GCs. **L** The effect of *TAB2* knockdown on the proliferation of GCs. The scale bars in (**I**, **L**) are 200 μm.

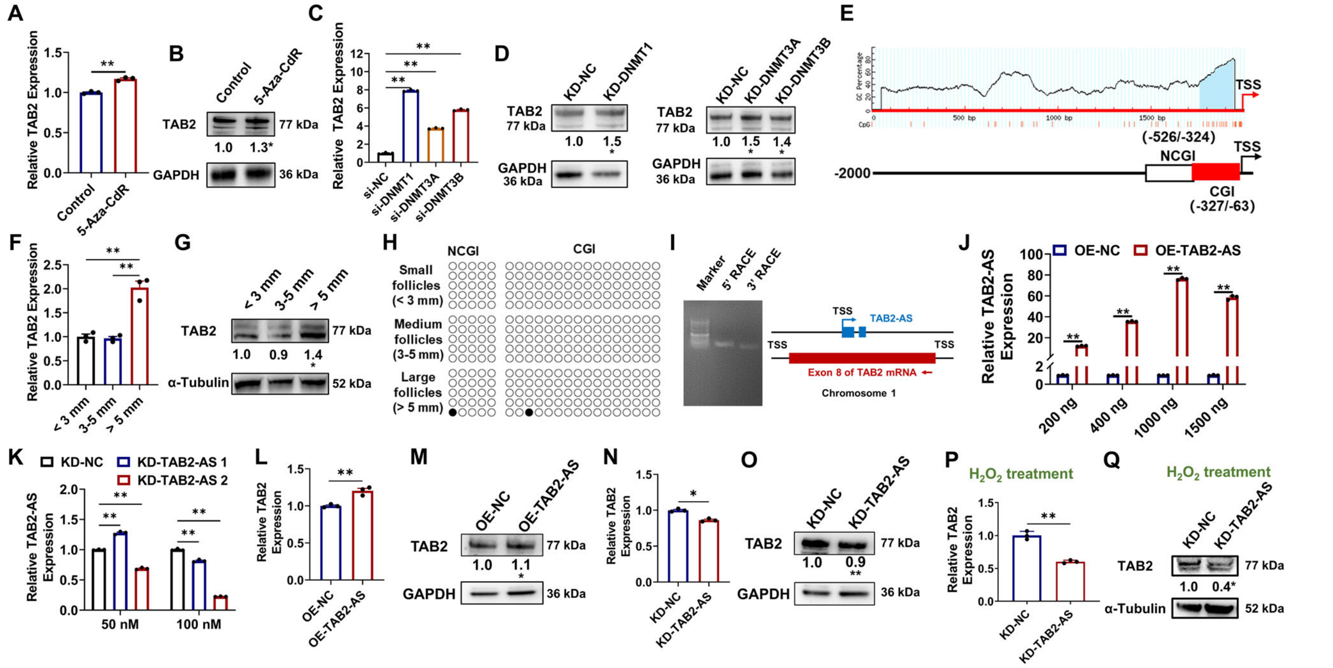

Fig. 3 | LncRNA *TAB2-AS*, an antisense RNA, is identified for *TAB2*. The mRNA (**A**) and protein (**B**) expressions of *TAB2* in GCs after treating by 5-Aza-CdR. The effects of *DNMTs* knockdown on the mRNA and protein (**D**) expressions of *TAB2*. (**E**) Schematic distribution of the CpG sites and bisulfite sequencing primers in the *TAB2* promoter. The mRNA (**F**) and protein (**G**) expressions of *TAB2* in small (< 3 mm), medium (3-5 mm), and large (> 5 mm) follicles. (**H**) The methylation status of CGI and NCGI of *TAB2* promoter in small, medium, and large follicles. (**I**) The identifications of *TAB2-AS* 5′ RACE and 3′ RACE. The overexpression (**J**) and knockdown (**K**) efficiencies of *TAB2-AS*. The mRNA (**L**) and protein (**M**) expressions of *TAB2* treated with *TAB2-AS* overexpression in GCs. The mRNA (**N**) and protein (**O**) expressions of *TAB2* treated with *TAB2-AS* knockdown in GCs. The mRNA (**P**) and protein (**Q**) levels of *TAB2* in GCs co-treated with H_2O_2 and *TAB2-AS* knockdown. CGI, CpG island; NCGI, non-CpG island.

knockdowns of DNA methyltransferase 1 (*DNMT1*), DNA methyltransferase 3 A (*DNMT3A*), and DNA methyltransferase 3B (*DNMT3B*) genes significantly promoted the mRNA (Fig. 3C) and protein (Fig. 3D) expressions of *TAB2*, suggesting DNA methylation might regulate the transcription of *TAB2*. Despite the mRNA (Fig. 3F) and protein (Fig. 3G) of *TAB2* expressed the highest in large follicles, compared to the small and medium follicles, and one CpG island (CGI, 265 bp, −327/−63 bp, transcription start site [TSS] = +1) resided in the promoter region of *TAB2* (Fig. 3E), but the CGI and non-CpG island (NCGI, 203 bp, −526/−324 bp) regions of *TAB2* were none methylated status in the small, medium, and large follicles (Fig. 3H). These observations suggested that DNA methylation did not directly regulate the transcription of *TAB2*. To further investigate the specific regulatory mechanism of DNA methylation in the expression of *TAB2*, we identified a lncRNA MSTRG 143.1 upregulated by 5-Aza-CdR based on RNA-seq[14]. MSTRG 143.1 was 241 nt in length, and located at the antisense strand of *TAB2* (Fig. 3I). We named MSTRG 143.1 as *TAB2* antisense RNA (*TAB2-AS*, submitting to GenBank with accession number OR554882) (Fig. 3I). Subsequently, we found that 1000 ng/mL overexpression vector and 100 nM antisense oligonucleotides 2 of *TAB2-AS* showed the strongest efficiency for the overexpression (OE-TAB2-AS) (Fig. 3J) and knockdown (KD-TAB2-AS) (Fig. 3K) of *TAB2-AS*, respectively. The mRNA (Fig. 3L) and protein (Fig. 3M) levels of *TAB2* in GCs were significantly enhanced after treating with *TAB2-AS* overexpression, while the *TAB2-AS* knockdown significantly inhibited the mRNA (Fig. 3N) and protein (Fig. 3O) expressions of *TAB2*. Moreover, the mRNA (Fig. 3P) and protein (Fig. 3Q) levels of *TAB2* were significantly decreased by knockdown of *TAB2-AS* in the GCs treated with H_2O_2.

DNA methylation mediated *TAB2-AS* to promote the expression of *TAB2*

Interestingly, *TAB2-AS* was found to express earlier than *TAB2* in GCs from 12 h to 30 h (Fig. 4A), during which GCs fully adhered to plate and began to proliferate[34]. This observation suggested that *TAB2-AS* might activate the transcription of *TAB2*. Using the specific ChIRP probes of *TAB2-AS*, we found that *TAB2-AS* significantly bound to *TAB2*'s mRNA (Fig. 4B) but not TAB2 protein (Fig. 4C). There were two overlap regions in the RNA sequence of *TAB2-AS* and *TAB2* (Fig. 4D). Subsequently, the overlap region 1 (OR1, 1–155 nt) and overlap region 2 (OR2, 156-241nt) of *TAB2-AS* sequence were cloned into pcDNA3.1 vector. The mRNA (Fig. 4E) and protein (Fig. 4F) levels of *TAB2* were increased significantly after overexpressing OR1 and OR2, suggesting that 1-155 nt and 156-241 nt of *TAB2-AS* were bound with 4368-4534 nt and 4215-4300 nt of *TAB2*'s mRNA, respectively. The CPC2.0 website predicted that *TAB2-AS* was a non-coding RNA (Protein-coding probability = 0.0125435) (Fig. 4G). To further explore the coding potential of *TAB2-AS*, the pcDNA3.1, pcDNA3.1-EGFP, pcDNA3.1-EGFP Mut, and pcDNA3.1-ORF-EGFP Mut vectors were constructed (Fig. 4H), and then transfected into GCs, respectively. The GCs transfected with pcDNA3.1-ORF-EGFP Mut vector didn't show EGFP fluorescence (Fig. 4I), indicating that *TAB2-AS* had no protein-encoding potential. Using FISH analysis (Fig. 4J) and nuclear mass separation assay (Fig. 4K), we identified that the enriched levels of *TAB2-AS* in the nucleus and cytoplasm of GCs were similar.

Besides, 5-Aza-CdR (Fig. 4L) and knockdowns of *DNMT1*, *DNMT3A*, and *DNMT3B* genes (Fig. 4M) significantly promoted the expression of *TAB2-AS*, which is similar to that of *TAB2*. Moreover, during the follicular growth, the expression of *TAB2-AS* increased gradually along with the expansion of follicular size (Fig. 4N). One CGI was identified in the promoter region of *TAB2-AS* (CGI, 222 bp, −1946/−1725 bp, TSS = +1; Fig. 4O). Compared to non-CGI region of *TAB2-AS* (NCGI, 281 bp, −2224/−1944 bp), the methylation levels of the CGI gradually decreased in the development of follicles (Small: 93.57%, Medium: 90%, Large: 88.57%). Especially, the methylation level of one CpG (−1759/−1760) were markedly changed. along with the expansion of follicular size (Fig. 4P), and 5-Aza-CdR seemed to markedly decrease the methylation levels of this CpG

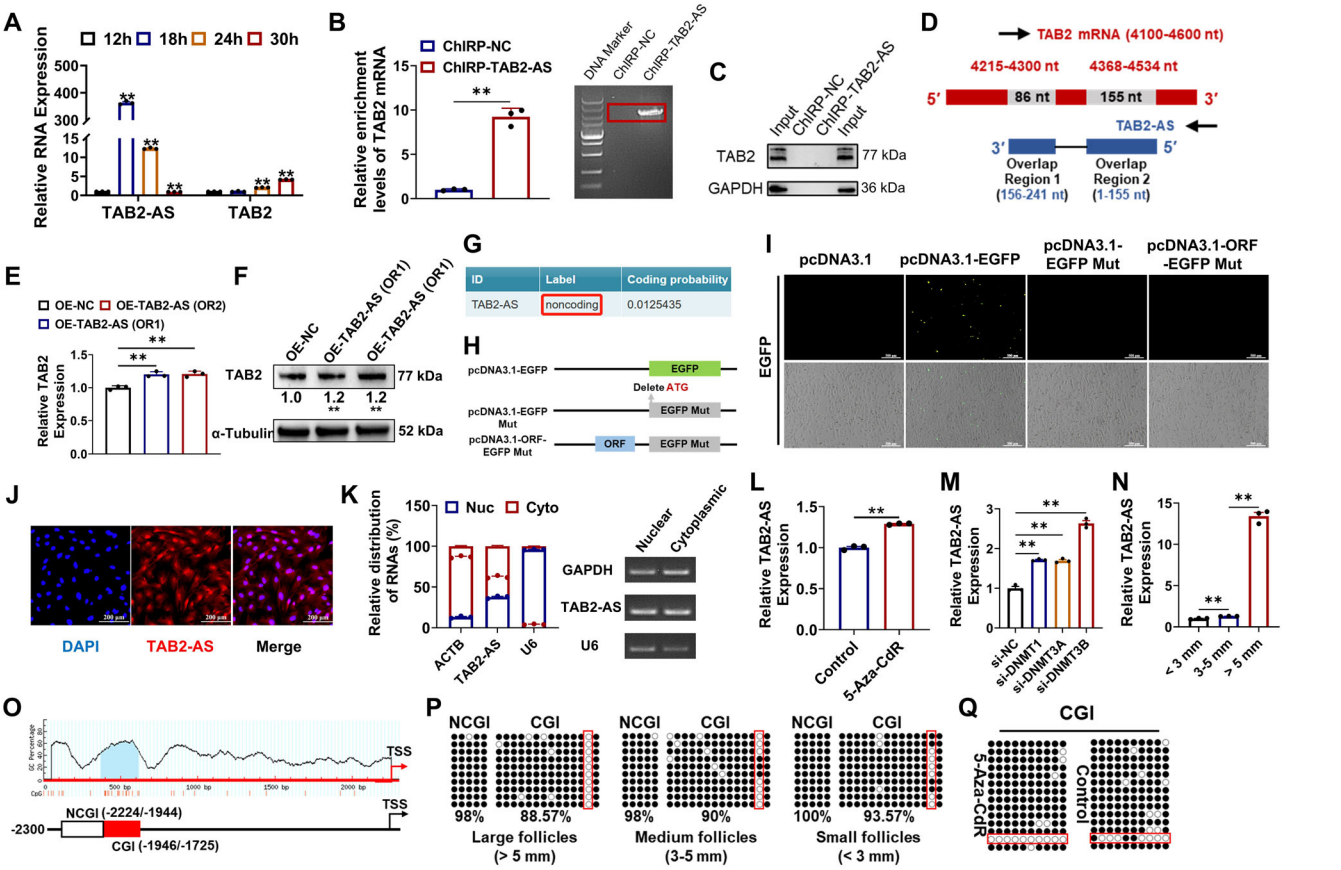

Fig. 4 | DNA methylation mediates *TAB2-AS* to promote the expression of *TAB2* via complementary to *TAB2*'s mRNA. A The mRNA expressions of *TAB2-AS* and *TAB2* at 12 h, 18 h, 24 h, and 30 h of cultured GCs. The binding status of *TAB2-AS* to mRNA (**B**) and protein (**C**) of *TAB2*. The Input and ChIRP-NC were selected as positive and negative controls, respectively. **D** Schematic diagram of the overlap regions between *TAB2-AS* and *TAB2* mRNA. The effects of OE-TAB2-AS (OR1) and OE-TAB2-AS (OR2) on the mRNA (**E**) and protein (**F**) expressions of *TAB2*. (**G**) The predicted results of protein-encoding ability for *TAB2-AS*. (**H**) The schematic diagram of EGFP fusion vectors. **I** The fluorescence signal of EGFP in the GCs transfected with fusion vectors. The FISH (**J**) and nucleoplasmic-qPCR (**K**) were used to identify the subcellular localization of *TAB2-AS*. Actin beta (*ACTB*) and *GAPDH* were used as cytosolic controls, and *U6* was used as nuclear control. The effects of 5-Aza-CdR treatment (**L**) and *DNMTs* knockdowns (**M**) on the expression of *TAB2-AS*. **N** The expressions of *TAB2-AS* in small, medium, and large follicles. **O** Schematic distribution of the CpG sites and bisulfite sequencing PCR (BSP) primers in the *TAB2* promoter. **P** The methylation status of the CGI and NCGI of *TAB2-AS* promoter in small, medium, and large follicles. **Q** The CGI methylation state in the GCs treated with 5-Aza-CdR. The scale bars in (**I**) are 500 μm, and the scale bars in (**J**) are 200 μm.

(−1759/−1760) (Fig. 4Q). Therefore, the methylation of CpG (−1759/−1760) was speculated to inhibit the transcription of *TAB2-AS*.

TAB2-AS inhibits the OS and apoptosis but promotes the proliferation of GCs via targeting *TAB2*

The mRNA (Fig. 5A) and protein (Fig. 5B) expressions of *SOD1*, *P50*, and *P65* in GCs were obviously increased by *TAB2-AS* overexpression. Meanwhile, *TAB2-AS* overexpression significantly inhibited the ROS accumulation of GCs (Fig. 5C). The *TAB2-AS* knockdown significantly decreased the mRNA (Fig. 5D) and protein (Fig. 5E) levels of *SOD1*, *P50*, and *P65* in GCs, and promoted the ROS accumulation of GCs (Fig. 5F). The *TAB2-AS* overexpression observably inhibited the mRNA (Fig. 5G) and protein (Fig. 5H) expressions of *Caspase-9* and *BIM*, and then inhibited the apoptosis of GCs (Fig. 5I). Conversely, *TAB2-AS* knockdown significantly promoted the mRNA (Fig. 5J) and protein (Fig. 5K) expressions of *Caspase-9* and *BIM*, and promoted the apoptosis of GCs (Fig. 5L). We found that the *TAB2-AS* overexpression significantly enhanced the expressions of *PCNA* and *CCNE1* (Fig. 6A, B) to promote the proliferation of GCs (Fig. 6C), while *TAB2-AS* knockdown suppressed the expressions of *PCNA* and *CCNE1* (Fig. 6D, E) to inhibit the proliferation of GCs (Fig. 6F). Notably, *TAB2* knockdown inhibited the proliferation of GCs treated by *TAB2-AS* overexpression (Fig. 6G), and promoted the apoptosis of GCs treated by *TAB2-AS* overexpression (Fig. 6H). Similarly, *TAB2* overexpression partially weaken the effects of *TAB2-AS* knockdown on the proliferation (Fig. 6I) and apoptosis (Fig. 6J) of GCs. It was likely that *TAB2-AS* regulated the OS, apoptosis, and proliferation of GCs via inducing the expression of *TAB2*.

TAB2-AS promotes follicular growth and sexual maturity

To further explore the biological function of *TAB2-AS* in follicular growth, the rLV-TAB2-AS or sh-TAB2-AS was infected into cultured porcine follicles. We found that the rLV-TAB2-AS significantly promoted the mRNA expressions of *TAB2*, *PCNA*, *SOD1*, *P65*, and *P50* in follicles, and significantly inhibited the mRNA expressions of *Caspase-9* and *BIM* in follicles (Fig. 7A). The sh-TAB2-AS showed the opposite results (Fig. 7A). Meanwhile, the rLV-TAB2-AS obviously upregulated the protein levels of PCNA, SOD1, P65, and P50, while obviously downregulated the protein levels of Caspase-9 and BIM (Fig. 7B). The opposite results were observed with sh-TAB2-AS (Fig. 7B). The apoptosis of GCs in follicles was markedly resisted by rLV-TAB2-AS, while the sh-TAB2-AS enhanced the apoptosis of follicular GCs (Fig. 7C). Besides, rLV-TAB2-AS inhibited the loss of follicular blood vessels and the opacity of follicular fluid, while the opposite results were observed by sh-TAB2-AS (Fig. 7D). We identified the expression of *TAB2-AS* in mouse ovarian via FISH analysis (Fig. 7E). Subsequently, rLV-TAB2-AS or sh-TAB2-AS was infected into mouse ovaries using intraperitoneal injection. The rLV-TAB2-AS significantly increased the mRNA levels of *PCNA*, *CCNE1*, *P50*, and *P65*, while sh-TAB2-AS significantly

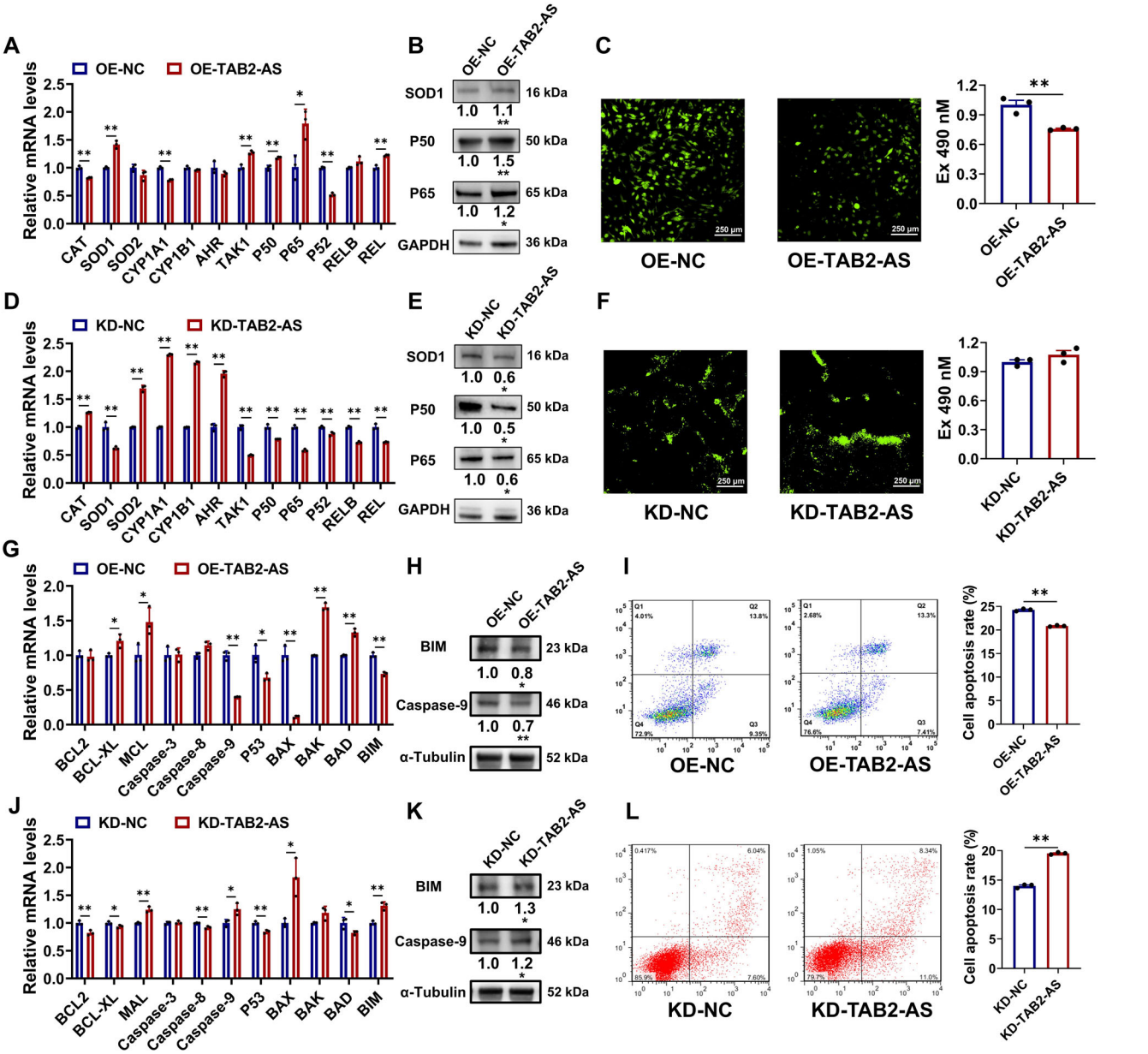

Fig. 5 | *TAB2-AS* inhibits the oxidative stress and apoptosis of GCs. The mRNA (**A**) and protein (**B**) expressions of several OS-related and NF-κB pathway genes in GCs after overexpression of *TAB2-AS*. **C** The effect of *TAB2-AS* overexpression on the ROS accumulation in GCs. The mRNA (**D**) and protein (**E**) expressions of several OS-related and NF-κB pathway genes after knockdown of *TAB2-AS* in GCs. **F** The effect of *TAB2-AS* knockdown on the ROS accumulation in GCs. The effects of *TAB2-AS* overexpression on the mRNA (**G**) and protein (**H**) expressions of apoptosis-related genes as well as the apoptosis levels (**I**) of GCs. The effects of *TAB2-AS* knockdown on the mRNA (**J**) and protein (**K**) expressions of apoptosis-related genes as well as the apoptosis levels (**L**) of GCs. The scale bars in (**C**) and (**F**) are 250 μm.

decreased the mRNA levels of *TAB2*, *PCNA*, and *P50* (Fig. 7F). Meanwhile, rLV-TAB2-AS enhanced the protein expression of P65, and sh-TAB2-AS reduced the protein expressions of TAB2, PCNA, and P65 (Fig. 7G). We found that the rLV-TAB2-AS induced the mouse ovaries to spawn more corpus luteum (Fig. 7H). Compared to the control group, lesser corpus luteum and more antral follicles appeared in the ovaries of mice with sh-TAB2-AS (Fig. 7H). These findings indicated that *TAB2-AS* promoted follicular growth and ovulation of mouse. The secretion of E2 was significantly upregulated by rLV-TAB2-AS, while sh-TAB2-AS reduced the secretion of estrogen (E2) in mouse serum (Fig. 7I). Furthermore, the sexual maturity of mice was advanced and delayed by rLV-TAB2-AS and sh-TAB2-AS, respectively (Fig. 7J). The litter size of mice with rLV-TAB2-AS was significantly increased compared to control group, while the sh-TAB2-AS obviously decreased the litter size of mice (Fig. 7K).

Discussion

The excessive mitochondrial redox reaction causes OS of GCs to induce follicular injury and ovarian diseases, including human premature ovarian insufficiency[35,36] and polycystic ovarian syndrome[37,38]. In mice, the excess ROS in ovarian GCs induced by FSH inhibits the normal follicular growth and leads to follicular atresia[39]. Furthermore, the activation of NF-κB signaling pathway is necessary for the growth of follicles in mammalian ovaries[40]. In this study, we significantly induced the OS in GCs using H_2O_2 treatment. Notably, there was no significant difference between GCs treated with 100 μM and 200 μM of H_2O_2 in the level of OS (Fig. 1A), indicating that there was no dosage-dependent of H_2O_2 on the induction of OS in GCs. Moreover, the expression of *TAB2* was downregulated in GCs treated by H_2O_2 (Fig. 1B, C). *TAB2* enhanced the expressions of *P50*, *P65*, and *SOD1* in GCs, and decreased the ROS accumulation of GCs (Fig. 1H–N). These results

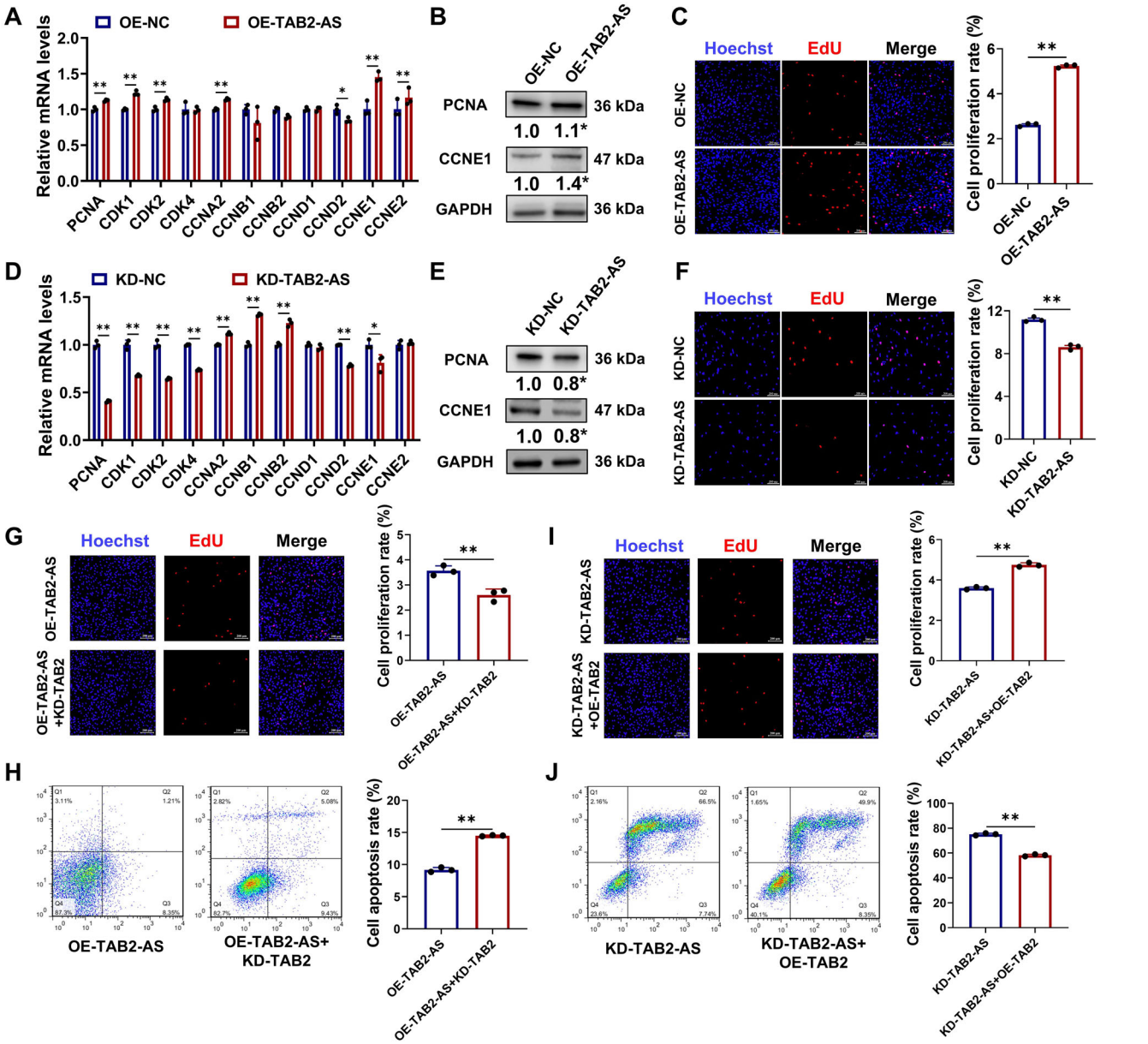

Fig. 6 | *TAB2-AS* promotes the proliferation of GCs. The mRNA (**A**) and protein (**B**) expressions of proliferation-related genes as well as the proliferation levels (**C**) of GCs treated with *TAB2-AS* overexpression. The mRNA (**D**) and protein (**E**) expressions of proliferation-related genes as well as the proliferation levels (**F**) of GCs treated with *TAB2-AS* knockdown. The effects of *TAB2* knockdown on the proliferation (**G**) and apoptosis (**H**) of GCs treated with *TAB2-AS* overexpression. The effects of *TAB2* overexpression on the proliferation (**I**) and apoptosis (**J**) of GCs treated with *TAB2-AS* knockdown. The scale bars in (**C**, **F**, **G**, **I**) are 200 μm.

indicated that *TAB2* inhibited the OS of GCs, and activated the NF-κB signaling pathway in GCs. The excessive apoptosis of GCs breaks the follicular growth and causes follicular atresia in mammalian ovaries[41]. For example, the ROS stimulates oxidative injury to facilitate the apoptosis of GCs in human ovaries[42]. In our study, *TAB2* significantly inhibited the apoptosis (Fig. 2A–F) and promoted the proliferation (Fig. 2G–L) of GCs. The change in amount of protein in the treatment groups was restricted, compared with control groups. We considered that the slight change in the amount of multiple protein regulated the functions of GCs. Collectively, *TAB2* inhibited the apoptosis of GCs via reducing the OS of GCs, and stimulated the proliferation and NF-κB signaling pathway of GCs. Notably, the GO and KEGG analyses showed that the differentially expressed genes between KD-NC and KD-TAB2 were enriched in follicular growth-related pathways, such as TNF signaling[43], PPAR signaling[44], and Estrogen signaling[45] (Fig. 1P, Q). These results indicated the biological targets of *TAB2* were diverse during the regulation of follicular growth, rather than being limited to OS of GCs.

DNA methylation medicates the expressions of genes in ovarian GCs via regulating the activity of gene promoter[46,47], and plays a pivotal factor to control follicular growth of mammals[48,49]. In mice, the genomic DNA of proliferating GCs occurs large-scale demethylation, and the expression of *DNMT1* appears decline in GCs during follicular development of ovaries[50]. We found that the expression of *TAB2* was upregulated in ovarian GCs treated by 5-Aza-CdR (Fig. 3A, B) and *DNMTs* knockdowns (Fig. 3C, D). Unexpectedly, the CGI and NCIG in promoter region of *TAB2* was virtually unmethylated (Fig. 3H). Subsequently, lncRNA *TAB2-AS*, an antisense RNA of *TAB2* was identified based on previous RNA-seq data[14] (Fig. 3I). Similar to protein-coding genes, the transcriptions of lncRNAs are also regulated by DNA methylation[51,52]. The expression of *TAB2-AS* was increased significantly in GCs treated with 5-Aza-CdR (Fig. 4L). With the expansion of follicular size, the expression of *TAB2-AS* was significantly increased (Fig. 4N), while the methylation levels of CpG (-1759/-1760) in *TAB2-AS* promoter was declined gradually (Fig. 4P). Interestingly,

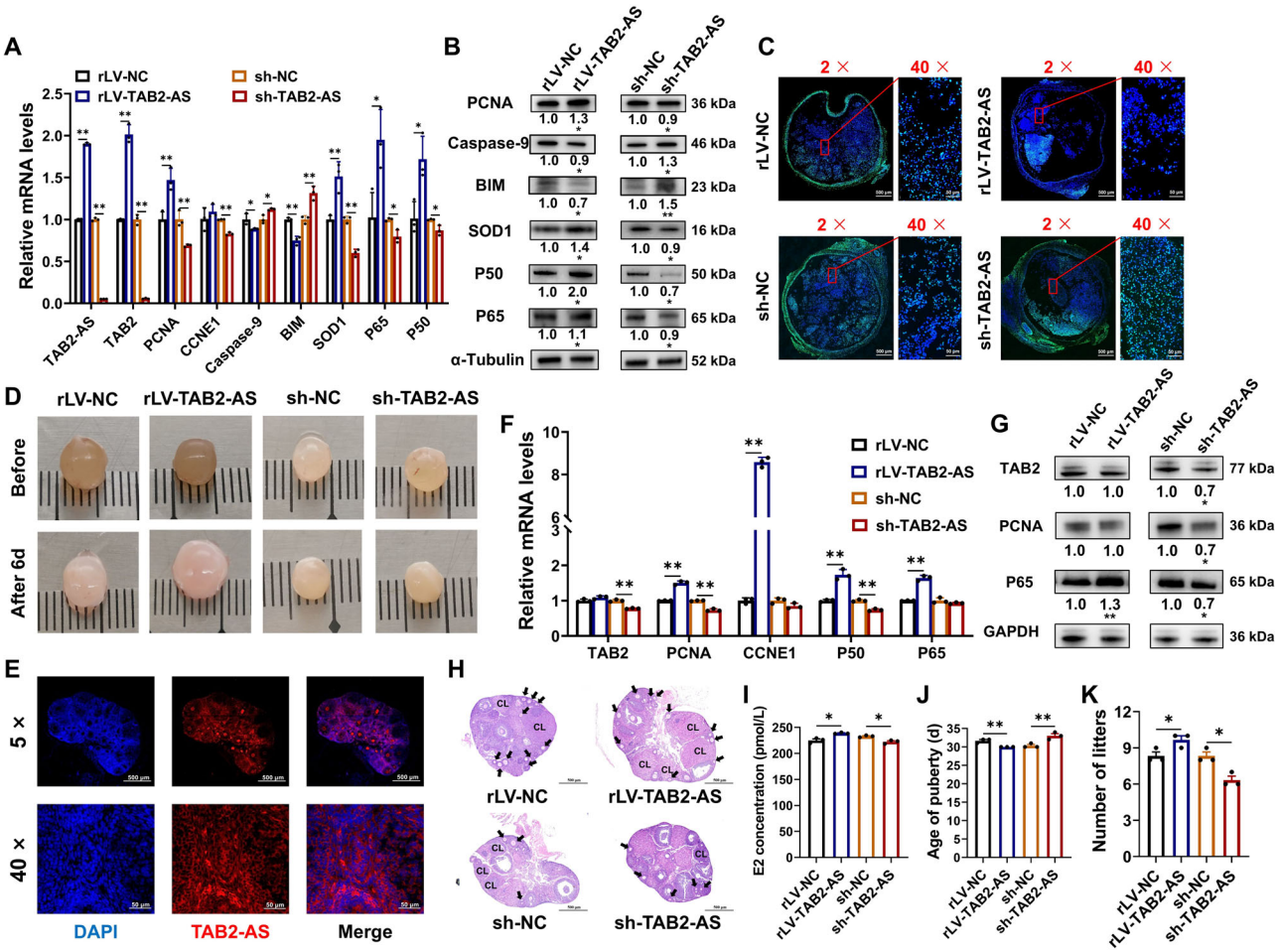

Fig. 7 | *TAB2-AS* promotes follicular growth and sexual maturity in vivo. A The RNA expressions of *TAB2-AS*, *TAB2*, *PCNA*, *CCNE1*, *Caspase-9*, *BIM*, *SOD1*, *P65*, and *P50* in the follicles treated with rLV-TAB2-AS and sh-TAB2-AS. **B** The protein levels of PCNA, Caspase-9, BIM, SOD1, P65, and P50 in the follicles treated with rLV-TAB2-AS and sh-TAB2-AS. **C** The follicles treated with rLV-TAB2-AS and sh-TAB2-AS were staining by TUNEL to assess the apoptosis status of GCs. **D** The morphological pictures of follicles treated with rLV-TAB2-AS and sh-TAB2-AS. The precision of ruler is 1 mm. **E** The FISH analysis on the expression of *TAB2-AS* in ovaries of mouse. **F** The mRNA expressions of *TAB2*, *PCNA*, *CCNE1*, *P50*, and *P65* in the ovaries of mouse treated by rLV-TAB2-AS and sh-TAB2-AS. **G** The protein levels of TAB2, PCNA, and P65 in the ovaries of mouse treated by rLV-TAB2-AS and sh-TAB2-AS. **H** The HE staining of mouse ovary treated by rLV-TAB2-AS and sh-TAB2-AS. CL and arrows indicate corpus luteum and antral follicle, respectively. The effects of rLV-TAB2-AS and sh-TAB2-AS on the E2 concentration in serum (**I**), sexual maturity (**J**), and litter size (**K**) of mice.

5-Aza-CdR inhibited the methylation of CpG (-1759/-1760) (Fig. 4Q), and *DNMTs* knockdowns increased the expression of *TAB2-AS* (Fig. 4M), suggesting that the *DNMTs* involved the methylation of CpG (-1759/-1760). These results indicated that the hypomethylation of CpG (-1759/-1760) promoted the transcription of *TAB2-AS* to regulate the expression of *TAB2*.

More recently, it is worth noting that lncRNAs have been demonstrated to involve in follicular growth and diseases of ovaries through regulating target gene[53–55]. We demonstrated that *TAB2-AS* was expressed earlier than *TAB2* during the proliferation of GCs (Fig. 4A). Studies have shown that PXN antisense RNA 1 (*PXN-AS1*) enhances the expression of paxillin (*PNX*) via binding to the *PNX*'s mRNA[56], and the similar regulatory mechanism was discovered between AR-regulated long noncoding RNA 1 (*ARLNC1*) and androgen receptor (*AR*)[57]. Similarly, we found that 1-155 nt and 156-241 nt regions of *TAB2-AS* were bound respectively to the 4368-4534 nt and 4215-4300 nt of *TAB2*'s mRNA, thus promoting the expression of *TAB2* (Fig. 4B–F). *TAB2-AS* significantly inhibited the ROS accumulation (Fig. 5A–F) and apoptosis of GCs (Fig. 5G–L), while promoted the proliferation of GCs (Fig. 6A–F).

To further characterize the function of *TAB2-AS*, the lentivirus infection was performed. Previous studies have confirmed that the atretic follicles appear degeneration of blood vessels and turbidity of follicular fluid[58,59]. In porcine follicles, we found that *TAB2-AS* inhibited the apoptosis of GCs (Fig. 7C), the degeneration of blood vessels, and the turbidity of follicular fluid (Fig. 7D), suggesting that *TAB2-AS* inhibited the follicular atresia. Similarly, *TAB2-AS* facilitated the follicular growth (Fig. 7H), E2 secretion (Fig. 7I), sexual maturity (Fig. 7J), and litter size (Fig. 7K) of mouse. Therefore, we speculated that *TAB2-AS* accelerated the sexual maturity by promoting follicular growth. Physiologically, we believed that *TAB2* resisted OS to determine the fate of follicle selection. Strong expression of *TAB2* might guarantee the high antioxidant activity of GCs, while the GCs that express *TAB2* weakly might be the specific cells with low antioxidant activity. *TAB2* ensured the normal growth of follicles, but suppression of TAB2 induced follicular abnormalities via decreasing antioxidant activity. There may be some limitations in our study. The genome epigenetic modification widely regulates gene expression[60], but the DNA methylation analysis in this study had been limited in the promoter of *TAB2*. The chromatin accessibility assay and ChIP assay appear to provide more valuable insights to explore the mechanisms by which epigenetic modifications regulate *TAB2* expression. The potential function by which FSH and LH regulated follicular growth by changing the expressions of *TAB2* and *TAB2-AS* was ignored. Considering the effects of FSH and LH on ROS accumulation, we did not add FSH and LH into the culture system of GCs. Moreover, it was likely that *TAB2-AS* might be a potential enhancer RNA[61] mediated by DNA methylation to enhance the transcription of *TAB2*.

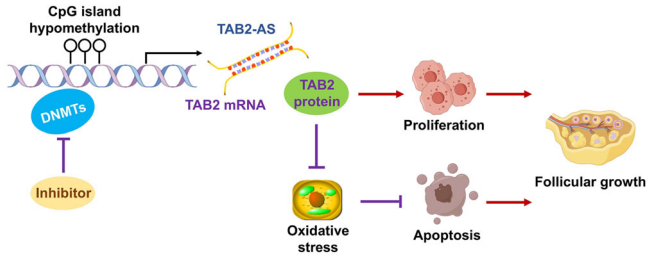

Fig. 8 | The mechanism diagram by which DNA methylation mediates *TAB2-AS* to promote follicular development via regulating the oxidative stress, apoptosis, and proliferation of GCs. The knockdown of *DNMTs* led to the hypomethylation of CGI in *TAB2-AS*'s promoter, thus enhancing the transcription of *TAB2-AS*. *TAB2-AS* bound with the 4215–4300 nt and 4368–4534 nt of *TAB2*'s mRNA to upregulate the mRNA and protein expressions of *TAB2*, which further inhibited the oxidative stress and apoptosis of GCs, promoted the proliferation of GCs, and ultimately ameliorated the follicular growth.

In conclusion, the *DNMTs* mediated *TAB2-AS* to promote the expression of *TAB2* via targeting the *TAB2*'s mRNA. The high expression of *TAB2* weakened the OS of GCs via activating NF-κB pathway to inhibit the apoptosis of GCs and promote the proliferation of GCs, ultimately expediting the growth of mammalian follicles (Fig. 8).

Methods

Cell culture

The of healthy porcine ovaries were cleaned twice with PBS containing 1% Penicillin-Streptomycin (Invitrogen, Shanghai, China) after collecting, and transported back to the laboratory at low temperature. The follicular fluid of 3–5 mm follicles was extracted using syringe, and centrifuged to separate the primary GCs. The GCs were resuspended in the Dulbecco's modified Eagle's medium (DMEM; Hyclone, Logan, UT, USA) containing 10% fetal bovine serum (Hyclone, Logan, UT, USA) and 1% Penicillin-Streptomycin (Invitrogen, Shanghai, China), and then incubated at 37 °C under 5% CO_2 after seeding into culture flasks The 3–5 mm follicles were peeled from ovaries by forceps and scalpels, and transferred to 24-well plates after washing twice with PBS. The collected follicles were cultured in serum-free DMEM/F12 medium, and incubated at 38.5 °C under 5% CO_2.

Quantitative reverse transcription PCR

The total RNA of cells and tissues were extracted using TRIzol reagent (TaKaRa, Tokyo, Japan), and then reverse-transcribed into cDNA using RevertAid First Strand cDNA Synthesis Kit (Thermo Scientific, Waltham, MA, USA). The Maxima SYBR Green qRT-PCR Master Mix (2×) (Thermo Scientific, Waltham, MA, USA) was used for cDNA quantification, according to the manufacturer's protocol. The relative expression levels of gene mRNAs were calculated with the $2^{-\Delta\Delta ct}$ method after measuring the CT value through CFX96 Touch Real-Time PCR system (Bio-Rad, Berkeley, CA, USA). Glyceraldehyde phosphate dehydrogenase (*GAPDH*) was served as the control gene. All primers for q-PCR are listed in Tables 1 and 2.

Transient transfection

Transfection was performed when GCs at high confluence (> 80%). The plasmid or oligonucleotide were transfected into GCs using Lipofectamine™ 3000 reagent (Thermo Scientific, Waltham). The GCs were cultured in Penicillin-Streptomycin-free medium during transfection. The modified minimal essential medium (Opti-MEM, Gibco, USA) was used to dilute liposome, plasmid, and oligonucleotide. The diluted liposome was incubated with diluted plasmid or oligonucleotide for 15 min at room temperature to prepare transfection solution. Finally, the transfection solution was added to cell medium and incubated for 5 h, and the original medium was replaced with medium containing 1% Penicillin-Streptomycin after cell transfection. All sequences of oligonucleotides are listed in Table 3.

Table 1 | Primers used for qPCR in pigs

Gene name	Primer sequences (5′ → 3′)	Size (bp)
LncRNA *TAB2-AS*	F: GGGCTGTAGGTACTGCTATTGTT R: GGTCACACTATATACTGACAGCAAC	132
TAB2 XM_013992499.2	F: GCTCACAGTCTTCTGCCCAT R: CTCCTGTGGTGGCATTAGCA	279
GAPDH NM_001206359.1	F: GGACTCATGACCACGGTCCAT R: TCAGATCCACAACCGACACGT	220
PCNA NM_001291925.1	F: GCAGAGCATGGACTCGTCTC R: TTGGACATGCTGGTGAGGTT	120
BCL2 XM_021099602.1	F: TTGCCGAGATGTCCAGCCAG R: TCAGTCATCCACAGGGCGAT	202
BCL-XL NM_214285.1	F: TGACCACCTAGAGCCTTGGA R: CGTCAGGAACCATCGGTTGA	124
MCL NM_001348806.1	F: GAAGGCGTTAGAGACCCTGC R: TGCCCCAGTTTGTTACTCCG	167
Caspase-3 NM_214131.1	F: GGATTGAGACGGACAGTGGG R: CCGTCCTTTGAATTTCGCCA	124
Caspase-8 XM_021074714.1	F: CTCTGCCTACAGGGTCATGC R: AGGATGGCCCTCTTCTCCAT	162
Caspase-9 XM_013998997.2	F: AACTTCTGCCATGAGTCGGG R: CTGGCCTTGGCAGTCAGG	128
P53 NM_213824.3	F: ACGCTTCGAGATGTTCCGAG R: TTTTATGGCGGGAGGGAGAC	137
BAX XM_013998624.2	F: AGCGCATTGGAGATGAACTG R: AAGTAGAAAAGCGCGACCAC	157
BAK XM_013977773.2	F: CTCGTCCACATCAGAGGAGC R: CTAGGTTCTAGGGGCAGGGT	147
BAD XM_021082883.1	F: AGTCGCCACTGCTCTTACCC R: TCTTGAAGGAACCCTGGAAATC	172
BIM NM_001252194.1	F: TTTGACACAGACAGGAGCCC R: AAGAAAACAGCATTACCCTCCT	226
CDK1 NM_001159304.2	F: AAGTGTGGCCAGAAGTGGAG R: CCAGAAATTCGCTTGGCAGG	157
CDK2 NM_001285465.1	F: TTTGCTGAGATGGTGACCCG R: GCTGAAATCCGCTTGTTGGG	254
CDK4 NM_00112309.7	F: GGCCCTCAAGAGCGTAAGAG R: GTCTCTCGATCAGTTCGGGC	165
CCNA2 NM_001177926.1	F: AACTTCAGCTTGTGGGCACT R: AACGAGGTGCTCCATTCTCA	140
CCNB1 NM_001170768.1	F: AGATCGCAGCAGGAGCTTTT R: CCTCGATTCACCACGACGAT	151
CCNB2 NM_001114282.1	F: AGCCACCCAGGTAGCTAAGA R: GAGAAGGACCCTTTGGAGCC	143
CCND1 XM_021082686.1	F: TTCATTTCCAACCCGCCCTC R: AGAAGGGCTTCGATCTGCTC	182
CCND2 NM_214088.1	F: AAGAGACCATTCCGCTGACG R: TTCTCATTGGGCTGAGGCAG	181
CCNE1 XM_005653265.2	F: GATGCGAAGGAACCTGACAC R: AGGAACAGGGGTTTTCACAGG	196
CCNE2 NM_001243931.1	F: TGACGGTCATCTCCTGGCTA R: CAGCAGCCGCCAGTATTCTA	177
CAT NM_214301.2	F: GCCGCCTATTTGCCTATCCT R: TCCCCAGAATAGCGGGTACA	226
SOD1 NM_001190422.1	F: CGAGCTGAAGGGAGAGAAGAC R: CTTGATCCTTTGGCCCACCA	170
SOD2 NM_214127.2	F: TGCAGCTCGAGCAGGAATCT R: CTTCTCCTCCACGACGTTCA	186
CYP1A1 NM_214412.1	F: CTGGGCACTTCGATCCCTAC R: AGTCACCTCCCCGAACTCAT	143
CYP1B1 XM_021087620.1	F: GCCAGCAGCGTGATGATTTT R: TGGGTTTAATGGTCAGGCCG	172
AHR NM_001303026.1	F: CAGCCGGACTCTCAGCATAG R: AAGTTCTGGCTTCTGACGGG	184

Table 1 (continued) | Primers used for qPCR in pigs

Gene name	Primer sequences (5′ → 3′)	Size (bp)
TAK1 NM_001114280.1	F: ATTCCAAGCCTAAACGGGGC R: GGATGACTTCGAGCTGGCTT	226
P50 NM_001048232.1	F: CCCTGGCGCATCTAGTGAAA R: TGCCTCTGTCATTCGTGCTT	274
P65 NM_001114281.1	F: CATGCGCTTCCGCTACAAG R: GGTCCCGCTTCTTTACACAC	284
P52 XM_021072741.1	F: GACAGTTGCTACGACCCACA R: CTGCTTAGGCTGTTCCACGA	144
RELB XM_021094520.1	F: TCGCCATCGTGTTCAAGACA R: TTCCGCTTCTTGTCCACTCC	166
REL XM_005662527.3	F: ATGTACACCGCCAAGTAGCC R: ACTCCACAATCCTGCCACAG	223

Table 2 | Primers used for qPCR in mouse

Gene name	Primer sequences (5′ → 3′)	Size (bp)
TAB2 XM_036155974.1	F: TCGCCAACTACTCCACAACC R: GACCTTGGGTTGACTACGGG	297
GAPDH NM_001289726.1	F: TGACCACAGTCCATGCCATC R: GACGGACACATTGGGGGTAG	203
PCNA NM_011045.2	F: GAACCTCACCAGCATGTCCA R: ATTCACCCGACGGCATCTTT	221
CCNE1 NM_007633.2	F: CTCCCACAACATCCAGACCC R: TGCTTCTTACTGCTGGGTGG	141
P50 NM_008689.2	F: CCCTACGGAACTGGGCAAAT R: GCGGAATCGAAATCCCCTCT	153
P65 NM_009045.5	F: GAGACCTGGAGCAAGCCATT R: CTGTCACCTGGAAGCAGAGG	123

Table 3 | List of oligonucleotides used in this study

Name	Sequences (5′ → 3′)
ASO-TAB2-AS	1. GTCAGTATATAGTGTGACCT 2. AAAGGGCTGTAGGTACTGCT
siRNA-TAB2	1. AAAGGGCTGTAGGTACTGCT 2. CCCATAGCCAATATAACAT 3. GGGTCCTGCCTTTATTCAT

Table 4 | Primers used for BSP

Primer name	Primer sequences (5′ → 3′)	Size (bp)
TAB2-AS-NCGI	F: TGGGTTTTAGATGAGGTTTAGATTT R: CAAACCACAAACTAATATCAATAAACTTTA	281
TAB2-AS-CGI	F: TTGATTTAGTTTGGTTATTTAAAAA R: AAACTATAACCACCAACCTAC	222
TAB2-NCGI	F: ATGTATATTTTGGATAGGGATAAAAA R: AAACCAAAAACACTTTAACTTAAAAC	203
TAB2-CGI	F: GTTTTGTTTTTAGGATTTTTAGGAA R: AAAAAAAACACACCCCCTTAAA	262

RNA-seq

The GCs treated with knockdown control (KD-NC) and *TAB2* knockdown (KD-TAB2) were used for RNA-seq, and four biological replicates were arranged for each group. The quality of total RNA extracted by TRIzol regen was detected by Nanodrop 2000 spectrophotometer (Thermo Scientific, USA) and gel electrophoresis. The ribosomal RNA (rRNA)-free total RNA was obtained using the RiboMinus™ Eukaryote Kit (Thermo Scientific, Waltham, MA, USA). The RNA sequencing was performed on the Illumina Hiseq 2500 platform (Illumina, San Diego, CA, USA) after building of rRNA-free total RNA libraries. The RNA reads were mapped to the Sus scrofa11.1 reference genome by HISAT2[62] and assembled by StringTie[63]. DESeq2[64] of R software was used for the identification of differentially expression genes (|log2FC| > log2 (1.5), *P*-value < 0.05) based on FPKM value.

Western blot assay and antibodies

The total protein of cells or tissues were extracted by RIPA buffer (Thermo Scientific, Waltham, MA, USA), and the concentration of total protein was detected using BCA reagent (BioSharp, Chengdu, China). The protein samples were added into 4-20% SDS polyacrylamide gel (Solarbio, Beijing, China) for electrophoresis. The eBlot™ L1 membrane converter (GenScript, Nanjing, China) was used to transfer the separated proteins to polyvinylidene fluoride (PVDF) membrane. The PVDF membranes were incubated with skim milk powder dissolved with Tris-buffered saline-Tween (TBST) for 2 h and then incubated with diluted primary antibodies at 4°C overnight. The information of primary antibody were as follows: anti-TAB2 (14410-1-AP, Proteintech, 1:3000), anti-GAPDH (10494-1-AP, Proteintech, 1:10000), anti-α-Tubulin (AF7010, Affinity, 1:5000), anti-PCNA (10205-2-AP, Proteintech, 1:2000), anti-CCNE1 (AF4713, Affinity, 1:2000), anti-Caspase-9 (AF6348, Affinity, 1:2000), anti-BIM (21280-1, Signalway, 1:1000), anti-P50 (21017, Signalway, 1:1000), anti-P65 (10745-1-AP, Proteintech, 1:3000), anti-SOD1 (10269-1-AP, Proteintech, 1:3000). The PVDF membranes were incubated with goat anti-rabbit IgG H&L (HRP) (ab150079, Abcam, 1:10000) at room temperature for 2 h. Finally, BCL color kit and the Odyssey Fc Imaging System (LI-COR Biosciences, Lincoln, USA) were used for visualization, and Image J software was used to analyze the gray value of protein. All unedited blot images are provided in Fig. S1.

Bisulfite sequencing PCR

The MethPrimer website (http://www.urogene.org/cgi-bin/methprimer/methprimer.cgi) was used to predict the CpG island of gene promoter and design the specific primer of BSP. The genomic DNA was extracted from follicular tissue by Tissue DNA Kit (D3396-02, Omega Bio-tek, USA). According to the manufacturer's protocol, the EZ DNA Methylation-GoldTM Kit (D5006, ZYMO RESEARCH, CA, USA) was used to convert the unmethylated cytosine of DNA sequence to uracil. Using the bisulfite-converted DNA as template, the corresponding fragments were amplified by BSP specific primer. Finally, the bisulfite-converted DNA fragments were sequenced, and then compared with the original sequences via the QUMA website (http://quma.cdb.riken.jp/). All primers for Bisulfite sequencing PCR are listed in Table 4.

EdU assay

The GCs were cultured in a 48-well cell culture plates. 48 h after GCs were transfected with plasmid or oligonucleotide, the Cell-LightTM EdU Apollo 567 In Vitro Kit (RiboBio, Guangdong, China) was used to analyze GCs proliferation. Briefly, the GCs were incubated with 50 μM EdU solution at 37°C for 2 h, and then fixed with 80% acetone after washing twice with PBS. The GCs were permeated by 0.5% Triton X-100 solution, and then incubated with 1× Apollo solution and 1× Hoechst for 30 min in darkness, respectively. Finally, the Nikon ECLIPSE Ti2 fluorescence microscope was used to collected the images of EdU positive cells (red) and Hoechst positive cells (blue).

Flow cytometry

The GCs were transfected with plasmid or oligonucleotide for 48 h before flow cytometry was performed, and three independent biological replicates were set for each experimental group. The apoptosis of GCs was detected using Annexin V-FITC Apoptosis Detection Kit (BioVision, Milpitas, CA, USA). The GCs were collected and washed twice with cold PBS. Subsequently, 5 μL Annexin V-FITC and 5 μL PI staining solution were added to GCs, and incubated 15 min in darkness. Finally, the flow cytometry (BD, USA) and Flowjo software were used to analyze the apoptosis rates of GCs. The Annexin V single positive GCs and Annexin V-PI double positive GCs were considered as viable apoptotic cells and non-viable apoptotic cells, respectively. The flow cytometry gating strategy is provided in Fig. S2.

Detection of ROS

The 2.5×10^3 of GCs were seeded in each well of 96-well plate, and transfected with plasmids or oligonucleotides for 48 h. The GCs were washed twice by cold PBS, and incubated with 10 mM DCFH-DA (Beyotime Biotech, Shanghai, China) in the dark for 30 min at 37 °C. The intracellular DCFH was oxidized to produce DCF in the presence of ROS. The green fluorescence intensity caused by DCH reflected the levels of ROS accumulation. Finally, the fluorescence intensity of DCH was measured on the Synergy Neo2 Hybrid MultiMode Reader (BioTek, Vermont, USA), and then imaged using fluorescence microscope. All of the data were acquired through averaging the results from three independent biological replicates. Results were normalized by the fluorescence intensity of control group.

Chromatin Isolation by RNA Purification pull down assay

The binding mRNA and protein of *TAB2-AS* were identified using the Pierce™ Magnetic RNA Protein Pull-Down Kit (Thermo Scientific, Waltham, MA, USA) and specific ChIRP biotin probes (RiboBio, Guangdong, China). The GCs were lysed using standard lysate buffers, and then centrifuged at 1000 rpm for 5 min to collect the cell lysates. The magnetic beads were incubated with the biotin probes in RNA Capture Buffer after washing by 20 mM Tris reagent. Then, the biotin probes captured the binding mRNA and protein of *TAB2-AS* in cell lysates, and the magnetic stand was used to collect beads. Finally, the magnetic beads were eluted using Elution Buffer to collect the elution products for subsequent analysis.

RNA FISH assay

The subcellular localization of *TAB2-AS* in ovarian GCs was determined using the RNA Fluorescence In Situ Hybridization (FISH) Kit and probes (RiboBio, Guangdong, China). The GCs were seeded in 24-well plates for 24 h, and then fixed with 4% paraformaldehyde for 10 min. Subsequently, the 0.5% Triton X-100 was used to permeate GCs. The GCs were incubated with FISH Probe Mix (20 μM) overnight at 37 °C after blocking by pre-hybridization solution. The GCs was washed three times, stained by DAPI for 10 min at room temperature, and examined using fluorescence microscope.

5' and 3' RACE assays

The full-length sequence of *TAB2-AS* was obtained using the SMARTer RACE 5'/3' Kit (Takara, Japan). The total RNA of GCs was incubated with 1× *E. coli* Poly(A) Polymerase (New England BioLabs, USA) for 1 h at 37 °C to prepare Poly A + RNA. The Poly A + RNA was reverse-transcribed into RACE-Ready first-strand cDNA using 5'/3' CDS Primer and First-Strand Buffer. Subsequently, the specific primers of 5' RACE and 3' RACE were designed according the known sequence of *TAB2-AS*, respectively. The RACE Nested-PCR was performed using cDNA as template. Finally, the products of the 5'/3' RACE were cloned into the pMD18-T clone vector (Takara, Japan) and sequenced.

ELISA assay

The mouse E2 ELISA Kit (JINGMEI Biotech, Jiangsu, China) was used for the detection of E2 levels in the serum. All reagents of ELISA assay were balanced at room temperature for 1 h. The 50 μL of standards and 50 μL of samples were added into the 96-wells ELISA plate, respectively. The antibody was added to each well, and then incubated at 37°C for 1 h. Then 50 μl each of reagent A and B were added into each wells after cleaning, and incubated at 37°C for 15 min in dark. The microplate reader was used to measure the absorbance at 450 nm. The ELISA standard curve was drawn according to the absorbance of standard with different concentrations. Finally, the E2 concentration was calculated through standard curve.

Animals and lentivirus delivery

All experiments were conducted according to Regulations for the Administration of Affairs Concerning Experimental Animals issued by the Ministry of Science and Technology of the People's Republic of China (Revised in March 2017), and approved by the Institutional Animal Care and Use Committee of Guangdong Laboratory Animals Monitoring Institute (Approval ID: IACUC2021168). The 4-week-old female C57BL/6 J mice were selected as model of in vivo experiment. All mice were bought from the Animal Experiment Center of Guangdong Province (Guangzhou, Guangdong, China). Mice were divided into 4 groups (rLV-NC, rLV-TAB2-AS, sh-NC, sh-TAB2-AS) with 5 individuals in each group, and fed freely on standard mouse chow. The environment temperature and humidity of mouse room were controlled at 25 °C and 40%–70%, respectively, and the 12-h light/12-h dark cycle was executed in mouse room. The ovaries of mice were infected with lentiviral at a dosage of 1×10^7 TU through intraperitoneal injection. The injection was given once a week for 3 weeks, during which the pubertal initiation of mice was characterized by the opening of vaginal orifice. After 3 weeks, the mice were killed by cervical dislocation and the ovarian samples were collected. The lentiviral vectors were synthesized by Guangzhou Dongze (Guangzhou, China).

Follicular culture

The 3–5 mm follicles of similar size were peeled from porcine ovaries by forceps and scalpels, and cleaned twice with PBS containing 1% Penicillin-Streptomycin (Invitrogen, Shanghai, China). The serum-free DMEM/F12 medium (Pricella, Wuhan, China) was used for follicular culture. Follicles were assigned into rLV-NC (n = 3), rLV-TAB2-AS (n = 3), sh-NC (n = 3), and sh-TAB2-AS ($n = 3$) groups, randomly. Subsequently, the follicles were incubated at 38.5 °C under 5% CO_2 after infecting with lentivirus at a titer of 1×10^6 TU for 6 days before imaged.

Mouse fertility assay

The female C57BL/6 J mice were divided into 4 groups (rLV-NC, rLV-TAB2-AS, sh-NC, sh-TAB2-AS) with 3 individuals in each group, and fed freely on breeding mouse chow. The lentivirus injection was given once a week for 3 weeks. Subsequently, each group of female C57BL/6 J mice that completed lentivirus injection were assigned one male C57BL/6 J mouse and mated, and the female mice were transferred to a separate cage after pregnancy until the offspring were born. The litter numbers of each female mice in the first litter were recorded and counted.

HE staining and TUNEL assay

The follicular growth and ovulation of mouse ovaries were analyzed through HE staining. The ovarian tissues were cut into maximum transverse sections after embedding in paraffin. Finally, sections were stained by HE. The apoptosis of GCs in follicles cultured in vitro were detected using a One Step TUNEL Apoptosis Assay Kit (Beyotime Biotech, Shanghai, China). The follicles were prepared into paraffin sections, and washed twice with cold PBS. Subsequently, the sections were treated by xylene, ethanol, and protease K, respectively. Finally, the follicular sections were incubated with TUNEL solution in the dark for 1 h, and the images were collected using fluorescence microscope.

Statistics and reproducibility

R software (R Software, USA) and GraphPad Prism 7.0 software (Chicago, IL, USA) were used to perform statistical analysis, and the unpaired t-test (two-tailed) was used to determine significant differences. All data are shown as mean value ± standard deviation (SD). The P-value < 0.05 or P-value < 0.01 was judged as the statistical significance. $^*P < 0.05$, $^{**}P < 0.01$.

The data of Western Blot were acquired through averaging the results from at least two independent biological replicates, and other data were acquired through averaging the results from three independent biological replicates.

Data availability

The RNA-seq data have been deposited in the Sequence Read Archive (SRA) database under accession number PRJNA1147792. All unedited blot/gel images and the flow cytometry gating strategy in this study have been included in Supplementary Information file. All data supporting of this study have been included in Supplementary Data file.

Received: 1 February 2024; Accepted: 25 September 2024;
Published online: 02 October 2024

References

1. Blasco, N. et al. Involvement of the mitochondrial nuclease EndoG in the regulation of cell proliferation through the control of reactive oxygen species. *Redox Biol.* **37**, 101736 (2020).
2. Jiang, L. et al. Dual-modal apoptosis assay enabling dynamic visualization of ATP and reactive oxygen species in living cells. *Anal. Chem.* **95**, 3507–3515 (2023).
3. Murphy, E. & Liu, J. C. Mitochondrial calcium and reactive oxygen species in cardiovascular disease. *Cardiovasc. Res.* **119**, 1105–1116 (2023).
4. Yamamoto, S. et al. Sunitinib with photoirradiation-mediated reactive oxygen species generation induces apoptosis of renal cell carcinoma cells. *Photodiagnosis Photodyn. Ther.* **35**, 102427 (2021).
5. Zhang, K. Y. et al. L-Selenocysteine induced HepG-2 cells apoptosis through reactive oxygen species-mediated signaling pathway. *Mol. Biol. Rep.* **49**, 8381–8390 (2022).
6. Liu, M. L. et al. Mitophagy and apoptosis mediated by ROS participate in AlCl3-induced MC3T3-E1 cell dysfunction. *Food Chem. Toxicol.* **155**, 112388 (2021).
7. Florido, J. et al. Melatonin drives apoptosis in head and neck cancer by increasing mitochondrial ROS generated via reverse electron transport. *J. Pineal Res*. **73**, e12824 (2022).
8. McGee, E. A. & Hsueh, A. J. W. Initial and cyclic recruitment of ovarian follicles. *Endocr. Rev.* **21**, 200–214 (2000).
9. Zhang, H. et al. Experimental evidence showing that no mitotically active female germline progenitors exist in postnatal mouse ovaries. *Proc. Natl Acad. Sci. USA* **109**, 12580–12585 (2012).
10. Manabe, N. et al. Regulation mechanism of selective atresia in porcine follicles: Regulation of granulosa cell apoptosis during atresia. *J. Reprod. Dev.* **50**, 493–514 (2004).
11. Zhang, J. B., Xu, Y. X., Liu, H. L. & Pan, Z. X. MicroRNAs in ovarian follicular atresia and granulosa cell apoptosis. *Reprod. Biol. Endocrinol.* **17**, 9 (2019).
12. Liang, J. Z. et al. Reactive oxygen species and ovarian diseases: Antioxidant strategies. *Redox Biol.* **62**, 102659–102659 (2023).
13. Akrami, R. et al. Comprehensive analysis of long non-coding RNAs in ovarian cancer reveals global patterns and targeted DNA amplification. *PLoS One* **8**, e80306 (2013).
14. Zhou, X. F. et al. DNMT1-mediated lncRNA IFFD controls the follicular development via targeting GLI1 by sponging miR-370. *Cell Death Differ.* **30**, 576–588 (2023).
15. Li, N. et al. A novel trans-acting lncRNA of ACTG1 that induces the remodeling of ovarian follicles. *Int J. Biol. Macromol.* **242**, 125170–125170 (2023).
16. Sun, D. et al. LncRNA DANCR counteracts premature ovarian insufficiency by regulating the senescence process of granulosa cells through stabilizing the interaction between p53 and hNRNPC. *J. Ovarian Res.* **16**, 41 (2023).
17. Yao, X. L. et al. lncRNA FDNCR promotes apoptosis of granulosa cells by targeting the miR-543-3p/DCN/TGF-beta signaling pathway in Hu sheep. *Mol. Ther. Nucleic Acids* **24**, 223–240 (2021).
18. Jones, P. A. Functions of DNA methylation: islands, start sites, gene bodies and beyond. *Nat. Rev. Genet* **13**, 484–492 (2012).
19. Yang, C. et al. The interaction between DNA methylation and long non-coding RNA during the onset of puberty in goats. *Reprod. Domest. Anim.* **53**, 1287–1297 (2018).
20. Li, J. et al. Epigenetic repression of long non-coding RNA MEG3 mediated by DNMT1 represses the p53 pathway in gliomas. *Int J. Oncol.* **48**, 723–733 (2016).
21. Tiane, A. et al. DNA methylation regulates the expression of the negative transcriptional regulators ID2 and ID4 during OPC differentiation. *Cell Mol. Life Sci.* **78**, 6631–6644 (2021).
22. Zhou, X. F. et al. DNA methylation mediated RSPO2 to promote follicular development in mammals. *Cell Death Dis.* **12**, 653 (2021).
23. Yuan, X. L. et al. Single-cell multi-omics profiling reveals key regulatory mechanisms that poise germinal vesicle oocytes for maturation in pigs. *Cell Mol. Life Sci.* **80**, 222 (2023).
24. Takaesu, G. et al. TAB2, a novel adaptor protein, mediates activation of TAK1 MAPKKK by linking TAK1 to TRAF6 in the IL-1 signal transduction pathway. *Mol. Cell* **5**, 649–658 (2000).
25. Jeffrey, K. L., Camps, M., Rommel, C. & Mackay, C. R. Targeting dual-specificity phosphatases: manipulating MAP kinase signalling and immune responses. *Nat. Rev. Drug Discov.* **6**, 391–403 (2007).
26. Xia, Q., Zhan, G. F., Mao, M., Zhao, Y. & Li, X. TRIM45 causes neuronal damage by aggravating microglia-mediated neuroinflammation upon cerebral ischemia and reperfusion injury. *Exp. Mol. Med* **54**, 180–193 (2022).
27. Pavlova, S., Klucska, K., Vasicek, D., Kotwica, J. & Sirotkin, A. V. Transcription factor NF-kappa B (p50/p50, p65/p65) controls porcine ovarian cells functions. *Anim. Reprod. Sci.* **128**, 73–84 (2011).
28. Gao, H., Lin, L., Ul Haq, I. & Zeng, S. M. Inhibition of NF-kappa B promotes autophagy via JNK signaling pathway in porcine granulosa cells. *Biochem Biophys. Res Commun.* **473**, 311–316 (2016).
29. Xu, J. J. et al. Role of nuclear factor-kappa B pathway in the transition of mouse secondary follicles to antral follicles. *J. Cell Physiol.* **234**, 22565–22580 (2019).
30. Peluso, J. J., Pru, C. A., Liu, X. F., Kelp, N. C. & Pru, J. K. Progesterone receptor membrane component 1 and 2 regulate granulosa cell mitosis and survival through a NF Kappa B-dependent mechanism. *Biol. Reprod.* **100**, 1571–1580 (2019).
31. Du, H. et al. Oxidative stress-induced lncRNA CYLD-AS1 promotes RPE inflammation via Nrf2/miR-134-5p/NF-κB signaling pathway. *FASEB J.* **36**, e22577 (2022).
32. Dong, W. X. et al. Ginsenoside Rb1 prevents oxidative stress-induced apoptosis and mitochondrial dysfunction in muscle stem cells via NF-κB pathway. *Oxid. Med Cell Longev.* **2022**, 9159101 (2022).
33. Ma, L. X. et al. Effects of TLR9/NF-κB on oxidative stress and inflammation in IPEC-J2 cells. *Genes genomics* **44**, 1149–1158 (2022).
34. Ren, K. N., Dai, W., Zhou, J. H., Su, J. & Wu, H. K. Whole-Teflon microfluidic chips. *Proc. Natl Acad. Sci. USA* **108**, 8162–8166 (2011).
35. Feng, P. H. et al. Study on the reparative effect of PEGylated growth hormone on ovarian parameters and mitochondrial function of oocytes from rats with premature ovarian insufficiency. *Front Cell Dev. Biol.* **9**, 649005 (2021).
36. Ding, C. Y. et al. Exosomal miRNA-320a is released from hAMSCs and regulates SIRT4 to prevent reactive oxygen species generation in POI. *Mol. Ther. Nucleic Acids* **21**, 37–50 (2020).
37. Gongadashetti, K., Gupta, P., Dada, R. & Malhotra, N. Follicular fluid oxidative stress biomarkers and ART outcomes in PCOS women undergoing in vitro fertilization: A cross-sectional study. *Int J. Reprod. Biomed.* **19**, 449–456 (2021).
38. Banuls, C. et al. Metabolic syndrome enhances endoplasmic reticulum, oxidative stress and leukocyte-endothelium interactions in PCOS. *Metabolism* **71**, 153–162 (2017).
39. Hoque, S. A. M., Umehara, T., Kawai, T. & Shimada, M. Adverse effect of superoxide-induced mitochondrial damage in granulosa cells on follicular development in mouse ovaries. *Free Radic. Biol. Med* **163**, 344–355 (2021).
40. Valdez, K. E. & Turzillo, A. M. Regulation of nuclear factor-kappa B (NF-kappa B) activity and apoptosis by estradiol in bovine granulosa cells. *Mol. Cell Endocrinol.* **243**, 66–73 (2005).
41. Zhang, H. Q. et al. Effects of hPMSCs on granulosa cell apoptosis and AMH expression and their role in the restoration of ovary function in premature ovarian failure mice. *Stem Cell Res Ther.* **9**, 20 (2018).
42. Yang, Z. W. et al. Chitosan oligosaccharides alleviate H2O2-stimulated granulosa Cell damage via HIF-1 alpha signaling pathway. *Oxid. Med Cell Longev.* **2022**, 4247042 (2022).

43. Duan, M. et al. Understanding heterogeneity of human bone marrow plasma cell maturation and survival pathways by single-cell analyses. *Cell Rep.* **42**, 112682 (2023).
44. Cui, Z. et al. Integrated Proteomic and Metabolomic Analyses of Chicken Ovary Revealed the Crucial Role of Lipoprotein Lipase on Lipid Metabolism and Steroidogenesis During Sexual Maturity. *Front Physiol.* **13**, 885030 (2022).
45. Ghorbani Ranjbary, A., Mehrzad, J., Talebkhan Garoussi, M. & Zohdi, J. Long Term Oral Administration of Oregano Essence Effectively Relieves Polycystic Ovarian Rats through Endocrine and Inflammatory Balance. *Evid.-based complementary alternative Med. : eCAM* **2022**, 5303583 (2022).
46. Mao, Z. R. et al. Methylome and transcriptome profiling revealed epigenetic silencing of LPCAT1 and PCYT1A associated with lipidome alterations in polycystic ovary syndrome. *J. Cell Physiol.* **236**, 6362–6375 (2021).
47. Sagvekar, P., Kumar, P., Mangoli, V., Desai, S. & Mukherjee, S. DNA methylome profiling of granulosa cells reveals altered methylation in genes regulating vital ovarian functions in polycystic ovary syndrome. *Clin. Epigenetics* **11**, 61 (2019).
48. Pan, Z. X. et al. Current advances in epigenetic modification and alteration during mammalian ovarian folliculogenesis. *J. Genet Genomics* **39**, 111–123 (2012).
49. Liu, Y. N. et al. DNA methylation in polycystic ovary syndrome: Emerging evidence and challenges. *Reprod. Toxicol.* **111**, 11–19 (2022).
50. Kawai, T., Richards, J. S. & Shimada, M. Large-scale DNA demethylation occurs in proliferating ovarian granulosa cells during mouse follicular development. *Commun. Biol.* **4**, 1334 (2021).
51. Chen, E. Z. et al. A genome-wide screen for differentially methylated long noncoding RNAs identified that lncAC007255.8 is regulated by promoter DNA methylation in Beas-2B cells malignantly transformed by NNK. *Toxicol. Lett.* **346**, 34–46 (2021).
52. Lee, E. Y., Song, J. M., Kim, H. J. & Park, H. R. Hypomethylation of lncRNA H19 as a potential prognostic biomarker for oral squamous cell carcinoma. *Arch. Oral. Biol.* **129**, 105214 (2021).
53. Geng, X. Y. et al. lnc-MAP3K13-7:1 inhibits ovarian GC proliferation in PCOS via DNMT1 downregulation-mediated CDKN1A promoter hypomethylation. *Mol. Ther.* **29**, 1279–1293 (2021).
54. Yao, W. et al. SMAD4-induced knockdown of the antisense long noncoding RNA BRE-AS contributes to granulosa cell apoptosis. *Mol. Ther. Nucleic Acids* **25**, 251–263 (2021).
55. Zhu, H. S., Chen, Y. Q. & Zhang, Z. F. Downregulation of lncRNA ZFAS1 and upregulation of microRNA-129 repress endocrine disturbance, increase proliferation and inhibit apoptosis of ovarian granulosa cells in polycystic ovarian syndrome by downregulating HMGB1. *Genomics* **112**, 3597–3608 (2020).
56. Yuan, J. H. et al. The MBNL3 splicing factor promotes hepatocellular carcinoma by increasing PXN expression through the alternative splicing of lncRNA-PXN-AS1. *Nat. Cell Biol.* **19**, 820 (2017).
57. Zhang, Y. J. et al. Analysis of the androgen receptor-regulated lncRNA landscape identifies a role for ARLNC1 in prostate cancer progression. *Nat. Genet* **50**, 814 (2018).
58. Lin, P. & Rui, R. Effects of follicular size and FSH on granulosa cell apoptosis and atresia in porcine antral follicles. *Mol. Reprod. Dev.* **77**, 670–678 (2010).
59. Barboni, B. et al. Vascular endothelial growth factor production in growing pig antral follicles. *Biol. Reprod.* **63**, 858–864 (2000).
60. Isbel, L. et al. Readout of histone methylation by Trim24 locally restricts chromatin opening by p53. *Nat. Struct. Mol. Biol.* **30**, 948–957 (2023).
61. Fang, K. et al. Cis-acting lnc-eRNA SEELA directly binds histone H4 to promote histone recognition and leukemia progression. *Genome Biol.* **21**, 269 (2020).
62. Kim, D., Langmead, B. & Salzberg, S. L. HISAT: a fast spliced aligner with low memory requirements. *Nat. Methods* **12**, 357–U121 (2015).
63. Pertea, M. et al. StringTie enables improved reconstruction of a transcriptome from RNA-seq reads. *Nat. Biotechnol.* **33**, 290 (2015).
64. Love, M. I., Huber, W. & Anders, S. Moderated estimation of fold change and dispersion for RNA-seq data with DESeq2. *Genome Biol.* **15**, 550 (2014).

Acknowledgements

This study was supported by grants from the Guangdong Basic and Applied Basic Research Foundation (2024B1515020112, 2023A1515010364, 2024A1515012999, 2023A1515030054, and 2022A1515012490), the National Natural Science Foundation of China (31902131 and 32072694), the Earmarked fund for China Agriculture Research System (CARS-35), and Breed Industry Innovation Park of Guangdong Xiaoerhua Pig (2022-4408×1-43010402-0019).

Author contributions

B.Y., H.Z., J.L., and X.Y. conceived the study. B.Y., N.L., and X.Y. designed experiments. N.L., B.Y., L.Z., Y.L., and Y.Z. performed in vitro experiments. M.F., S.L., Y.C., E.H., and L.Z. conducted in vivo experiments. N.L., B.Y., and X.Y. summarized results and wrote the paper with revising by N.L., B.Y., Y.J., and X.Y.

Competing interests

The authors declare no competing interests.

Additional information

Supplementary information The online version contains supplementary material available at https://doi.org/10.1038/s42003-024-06960-6.

Correspondence and requests for materials should be addressed to Jiaqi Li or Xiaolong Yuan.

Peer review information *Communications Biology* thanks Masayuki Shimada and the other, anonymous, reviewer for their contribution to the peer review of this work. Primary Handling Editors: Andrew Jobbins, Christina Karlsson Rosenthal and Kaliya Georgieva.